JOURNAL OF PROPULSION AND POWER
Vol. 25, No. 3, May–June 2009

Plume Profiles of a Planar Crossed-Field Thruster with Hall Current Injection

Joshua L. Rovey,* Matthew P. Giacomi,† Robert A. Stubbers,‡ and Brian E. Jurczyk§
Starfire Industries, LLC, Champaign, Illinois 61820

DOI: 10.2514/1.35720

Stable operation of a Hall thruster that emits and collects the Hall current across a planar discharge channel is described. Hall current was emitted by hollow cathode electron sources and collected by electrodes on the opposing wall of the thruster. During this initial test, the planar Hall thruster was operated at discharge voltages between 100–150 V. Internal channel wall probes, along with a downstream Faraday probe and retarding potential analyzer, measured changes in thruster plasma as the discharge voltage and magnetic field were adjusted. Results show that most of the plume ions were created in the acceleration zone and gain only 60–70% of the discharge voltage. Furthermore, the axial plume ion energy decreased with increasing magnetic field. Specifically, when the electromagnet was increased from 1.5 to 3.5 A, the ion energy decreased 25%. The plume current density profile showed a peak at 15–20 deg off-centerline, and this angle increased with increasing magnetic field. Specifically, when the electromagnet was increased from 1.5 to 3.5 A, the peak location shifted 4 deg farther from the centerline. Analysis of these results suggests that a buildup of Hall current electrons on one side of the discharge channel leads to a nonuniform plasma density. Further, magnetohydrodynamic effects on the expelled ion beam leads to cross-field ion velocity, resulting in the off-centerline peak in the current density profile.

Nomenclature

B	=	magnetic field strength
E_a	=	axial energy
E_r	=	cross-channel energy
I_{emag}	=	electromagnet current
L	=	cross-channel length
$Mdot_a$	=	anode mass flow rate
$Mdot_e$	=	total emitter mass flow rate
n	=	plasma density
n_b	=	background neutral density
n_o	=	initial plasma density
r_L	=	Larmor radius
T_e	=	electron temperature
V_a	=	anode voltage
v	=	ion velocity
W	=	high-B region width
x	=	cross-channel position
σ_{ei}	=	electron-impact ionization collision cross section

I. Introduction

HALL-EFFECT thrusters (HETs) are a type of space propulsion device that use electric fields to accelerate and expel ionized propellant to generate thrust. A schematic of an HET is shown in Fig. 1. A HET is a coaxial device that uses a radial magnetic field crossed with an axial electric field. Electrons emitted by the cathode drift in the ExB direction, forming an azimuthal Hall current. Neutral xenon atoms injected through the anode collide with these electrons, producing xenon ions that are subsequently accelerated by the electric field to produce thrust. The magnitude of the magnetic field is designed such that only the electrons are magnetized. A mixture of electrons and ions in the acceleration zone creates a quasi-neutral plasma, and thus the operation of the HET is not space-charge limited in ion current density as is the case with gridded ion thrusters.

Transverse electron mobility represents a loss in efficiency of the device, and so, ideally, electrons would be confined to drift in the Hall current indefinitely. Unfortunately, this is not realizable in practice and electrons do migrate to the anode. Furthermore, axial mobility cannot be characterized by a purely classical collisional diffusion model. In fact, experimental measurements in the Stationary Plasma Thruster-100 have shown that the electron collision frequency is on the order of 10^7–10^8 Hz [1]. Calculations from both internal and global measurements have shown that the collision frequency based off of classical theory is 1000 times lower [2]. Because of this discrepancy, the term "anomalous" mobility has been used to describe the increased axial mobility present in cross-field devices such as HETs [3]. Explanations of the anomalous mobility have been suggested, and two main candidates are plasma turbulence [2,4] and wall effects [5–7]. More efficient HETs that better confine Hall current electrons may be possible if a clearer understanding of the mobility in these devices is developed. In the present work, a planar Hall thruster (PHT) was investigated with the eventual goal of using the device as a test bed to study electron mobility in ExB devices.

Since the late 1960s, the only reported developments on a nonaxisymmetric Hall thruster configuration were at Stanford University and the University of Michigan [8–10]. The Stanford team developed the linear Hall device to readily test different secondary electron emitting materials that were impossible to fabricate in 2-D form, such as alumina or diamond. The linear device at Stanford reported highly localized heating on the ceramic in the direction of the ExB Hall drift, nonsymmetric discharges and ion plumes, and highly unstable or oscillatory operation across a range of operation.

In early 2001, the University of Michigan tested a two-stage version of the linear Hall thruster called the Linear Gridless Ion Thruster (LGIT) [9]. This system improved on the original diagnostic test stand at Stanford University, and was a fully fabricated thruster geometry with a separate ionization stage, in an attempt to improve efficiency by decoupling the ionization and acceleration processes. Only results for one single 3-min single-stage operation were reported in the literature, because the interior hollow anode ionization zone was not completed. It is important to note that the

Received 16 November 2007; revision received 8 April 2008; accepted for publication 28 June 2008.

*Propulsion Research Engineer; currently Assistant Professor of Aerospace Engineering, Missouri University of Science & Technology, Rolla, Missouri 65409. Member AIAA.
†Research Engineer. Member AIAA.
‡Vice President, 60 Hazelwood Drive, Suite 143/203A. Member AIAA.
§President. Member AIAA.

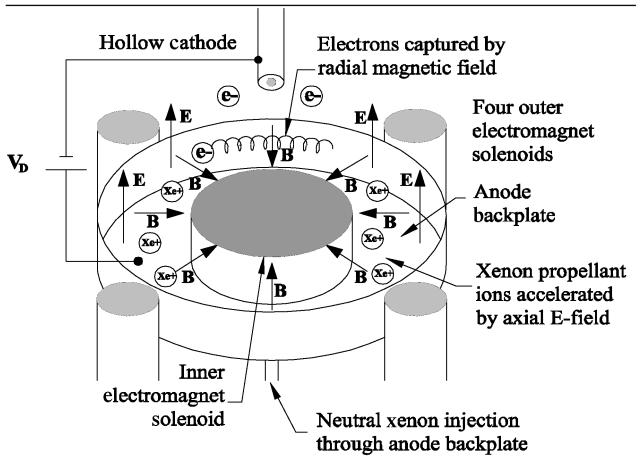

Fig. 1 Schematic of a traditional, annular Hall-effect thruster.

University of Michigan team included a drift current electrode to enable the collection of electrons transiting the device. This electrode was intended to prevent the buildup of space charge experienced in the Stanford University experiment and was placed across the acceleration region opposite the external hollow cathode dispenser. However, the placement of a single large electrode piece would completely short out the electric potential across the plasma acceleration region. This effect could explain the low thrust efficiency (∼14%) reported and device short leading to failure after a few minutes of operation. Although the test was not completely successful, it did demonstrate the operation of a linear Hall thruster configuration without a closed electron drift.

In the present work, a PHT that injects the Hall current into the discharge channel was investigated. As previously stated, the eventual goal is to use the device as a test bed to study electron mobility in crossed-field devices. The planar geometry attempts to decouple the complex electron motion found in annular thrusters by using a simplified geometry. Annular HETs are known to contain complex electron motions resulting from gradients in the magnetic field, curvature drifts, radial electric fields, and magnetic mirror phenomena [11,12]. These effects can lead to electron drifts, plasma instability, and wall cascades that limit device performance. The goal of the PHT is to remove some of the complexity resulting from the annular geometry to better study electron motion in *ExB* fields. The rectilinear design effectively eliminates the curvature-induced electron transport losses present in the annular system; however, there is the challenge of dealing with the accumulated Hall current because the system is not "closed drift." To solve this problem, the electron Hall current is injected into the acceleration region of the thruster through a port in the sidewall of the thruster channel ceramic. On the opposite side of the channel, a series of segmented electrodes capture the injected Hall current and recirculate this charge for reinjection on the opposite side.

Without emissive electrodes and collector electrodes across the channel, the PHT would be similar to the Stanford linear thruster and the Michigan LGIT. The magnetic field impedes electron motion to the anode, setting up an axial electric field in the high-*B* region, which accelerates ions to generate thrust. Electrons impeded by the magnetic field are also affected by the axial electric field and preferentially drift in the *ExB* direction, that is, the Hall current. In the linear or planar configuration, the Hall current is not closed and these electrons will likely impact the channel wall and cascade to the anode. This phenomenon was anticipated by the Michigan group with the LGIT device, and so they incorporated an electrode at the end of the channel to collect the Hall current [9]. The cross-channel emitter and collector electrodes of the PHT are present to adjust and recirculate this cross-channel Hall current, so that (ideally) the electrons do not impact the wall and cascade to the anode, but rather get collected (by the collector electrodes) and then reemitted on the opposite side of the channel.

The initial experiment presented here was designed to assess the operational stability and functionality of the PHT. Specific questions to be addressed were as follows:

1) Will the PHT geometry and setup produce a stable plasma discharge?

2) Can current be emitted and collected across the channel?

3) What is the shape of the thruster beam profile? The following sections describe the PHT experimental apparatus, results, and conclusions from this investigation.

II. Experimental Apparatus and Setup

A. Hall Thruster

The PHT does not have the annular shape of the conventional Hall thruster. Rather, the device is planar (or linear) and Hall current is emitted at a sidewall and collected at the other end after traveling across the channel. A schematic of the device is shown in Fig. 2. A photograph of the thruster before and during operation is shown in Fig. 3.

The discharge channel is constructed of baked alumina silicate ceramic plates. Its length, width, and depth are 203, 25, and 108 mm, respectively. The anode is placed at the back of the channel and the back channel plate is bolted to the main pole piece of the electromagnetic circuit. The magnetic circuit is made of standard low-carbon steel with a relative permeability of approximately 3000. The back (upstream) pole piece is a 12-mm-thick, 203 × 305 mm plate. Twelve 83-mm-long, 19-mm-diam posts were welded to the back pole piece and then wound in series with approximately 100 m of magnet wire. The front (downstream) pole pieces are bolted to the posts. The top and bottom front pole pieces are each 76 mm wide, 38 mm thick, and 305 mm long. Two grooves cut into each pole along their length and on the side facing the channel are used to obtain the desirable magnetic field geometry. Flux density measurements midway between the two front pole pieces yielded a magnetic field of approximately 60 G/A of electromagnet current. Furthermore, the front pole pieces extend farther laterally than the channel so that edge effects are minimized. There is no magnetic shield and no trim coils to adjust the shape of the magnetic field. These components have been used by other researchers to adjust both the shape and magnitude of the magnetic field in other HETs [11,13,14]. The field shape was constant and only the flux density magnitude was adjusted in this investigation. The stainless steel anode also serves as a gas manifold.

B. Channel Wall Emitter Cathodes

Hall-current is emitted on the side of the PHT by two hollow cathodes. Each cathode is a 6.4-mm-diam tantalum tube with a stainless steel gas connection and a shielded heater. The cathodes are inserted through the discharge channel wall and protruded into the channel approximately 1–3 mm. Xenon is used as the working gas. The heater coil increases the temperature of a tantalum emitter such that it thermionically emits electrons inside the cathode tube. Electrons are then dispensed through a small orifice approximately 3.2 mm in diameter. Electron extraction was provided by titanium collector plates on the opposite side of the thruster. The collectors are recessed into the discharge channel sidewall. There are two emitters

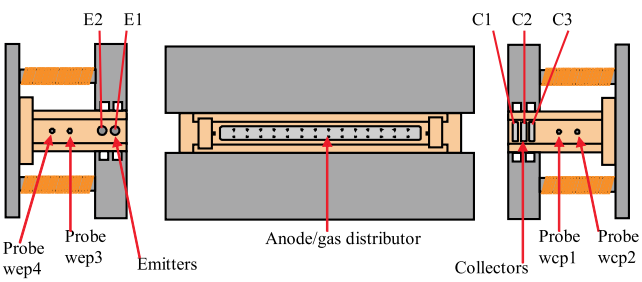

Fig. 2 Schematics of the PHT. The left picture shows the emitter side of the channel. The center picture looks into the channel. The right picture looks at the collector side of the thruster.

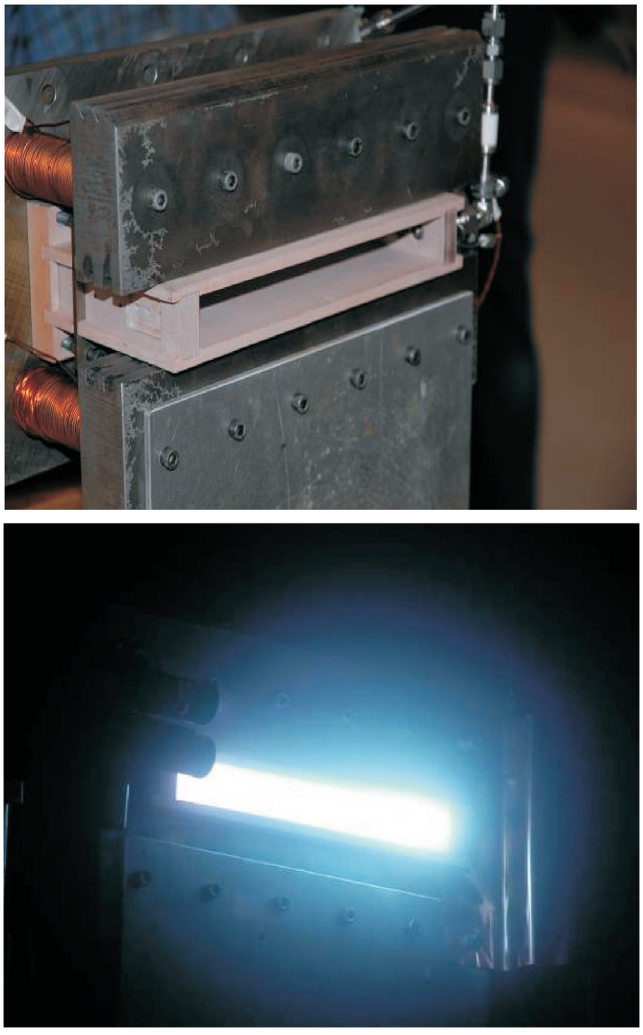

Fig. 3 PHT before (top) and during (bottom) operation in the vacuum test facility.

and three collector plates, and the two collector plates nearest to the anode are electrically connected to act as a single collector. The upstream emitter (emitter 2) is located 8.3 cm from the anode, whereas the downstream emitter (emitter 1) is 9.5 cm from the anode. For reference, the exit plane is 10.8 cm from the anode.

The emitter hollow cathodes are ignited by first supplying a current to the heater coil, which heats the insert to approximately 1000°C. Next, gas flow is supplied while a potential is applied between the cathode and a collector across the channel. This causes electrons to be thermionically emitted from the insert and then to interact with the gas flow, creating plasma inside the cathode tube. At this point, the cathode should become self-sustaining and the heater current can be eliminated because plasma ions recombine at the insert, depositing their energy and sustaining the cathode insert temperature required for electron emission. For this experiment, the heater was always energized to keep the cathode emitting. Electrons are pulled through the cathode orifice by the potential between the cathode and collector. Emitted electrons enter the discharge channel and Hall drift across the channel to the collector. A schematic of the electrical connections for PHT operation are given in Fig. 4.

C. Neutralizer Cathode

The neutralizer is a lanthanum hexaboride (LaB_6) hollow cathode flowing xenon. A mass flow rate of 8 sccm-Xe was typical. The heater current was constant at 8 A and the cathode-to-ground potential was generally between −5 and −10 V. The neutralizer is mounted on the collector side of the thruster approximately 5 cm to the side of the thruster and 10 cm downstream of the exit plane, as

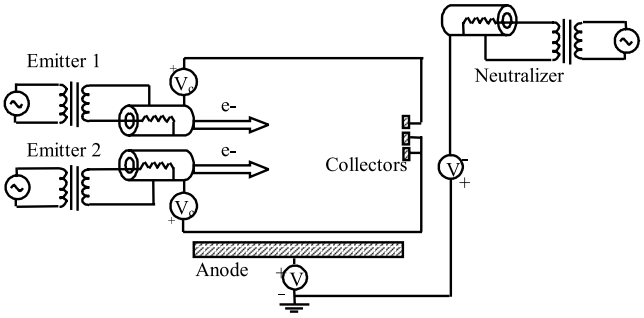

Fig. 4 Electrical schematic of PHT operation.

seen in Fig. 3. Two neutralizers were mounted, but only one was used.

D. Facility

The PHT was operated in chamber 3 at the U.S. Air Force Research Laboratory (AFRL). Chamber 3 is a stainless steel, cylindrical vacuum chamber 3.3 m in diameter by 8 m long. The thruster exit plane is located in the center of the chamber diameter, pointing down the long axis approximately 7 m from the far end. All surfaces that are optically visible to the plasma plume are shielded with $\frac{1}{2}$ in. thick, high-purity, sulfur-free carbon plates. A dedicated dry Stokes mechanical pump reaches rough vacuum with a pumping speed of 450 L/s, and a Pfeiffer vacuum turbomolecular pump removes lighter gases. The facility uses eight helium-cooled cryopanels, resulting in a maximum xenon pumping speed of 140,000 L/s. The heat load to these cryopanels is moderated by shrouds coated with low-emissivity paint, which are cooled by four IGC Polycold Cryogenic Refrigeration units. A conservative measurement of the ultimate base pressure is less than 1×10^{-7} torr. The chamber is equipped with a thrust stand, scanning Faraday probe, and retarding potential analyzer (RPA). The Faraday probe and RPA are mounted to a motor and rotate 180 deg around the thruster. For more information regarding the facility and pressure measurement, the reader is referred to [15].

E. Diagnostics

The plasma diagnostics used to study the PHT were an RPA, Faraday probe, and multiple channel wall probes. The channel wall probes were located inside the discharge channel of the thruster, whereas the RPA and Faraday probe were swept through the plume of the device at a distance of 1 m from the PHT exit plane. Furthermore, the voltage and current of all PHT components were also monitored to assess the operation of the device. The following sections describe the plasma probe diagnostics used in this investigation.

1. Retarding Potential Analyzer

An RPA is used to analyze ion voltage distributions downstream of the PHT. In an RPA, a series of biased grids selectively filter ions from reaching a current-measuring probe depending on their energy-to-charge ratios. Specifically, the derivative of the resulting I-V characteristic is proportional to the ion voltage distribution function [16]. Of primary importance for the research presented here is the voltage value for the peak in the distribution function, otherwise known as the most-probable voltage.

The RPA used for these experiments has four grids: floating, electron repelling, ion retarding, and electron suppression grids. The electron suppression grid was biased at a constant −15 V with respect to ground, whereas the electron repelling grid was biased to −30 V with respect to ground. RPA data are acquired on the centerline of the thruster and ion retarding grid voltage sweeps of 0–200 V were used because the discharge voltage was never greater than 150 V. More information regarding the RPA construction and the operation electronics have been described in previous papers [14,15].

2. Nude Faraday Probe

A Faraday probe is a type of plasma diagnostic that is often used to measure the ion beam current density profile of Hall thrusters. It consists of a planar metallic electrode that is biased negative so as to repel electrons. The probe is swept through the thruster plasma plume and current measurements are taken as a function of angular position. This procedure reveals the plume profile of the thruster. For the experiments presented here, the Faraday probe was a 19-mm-diam electrode surrounded by a 43-mm-diam annular guard ring. The guard ring surrounding the probe was used to establish a planar sheath and minimize edge effects. Both the probe and guard ring were biased at −20 V with respect to ground. Previous experiments have shown this to be sufficient for the probe to be in the ion saturation regime. Collected current was calculated by measuring the voltage drop across a 40.4 Ω shunt resistor and the corresponding current density was calculated by dividing by the probe area. More information regarding the nude Faraday probe can be found in [15].

3. Channel Wall Probes

The channel wall probes are made of 1-mm-diam tungsten wire. They are positioned 2.5 and 5 cm from the anode. Each probe fits snugly through a hole in the channel and protrudes 2 mm into the discharge volume. A schematic is shown in Fig. 5. These probes are used to measure the plasma floating potential at different locations within the discharge channel. In this experiment, no Langmuir probe traces were taken, only the floating potential was measured with respect to ground. The nomenclature for the probes is as follows. The upstream and downstream probes on the channel electron collector side are referred to as wall collector probes 2 and 1 (wcp2 and wcp1), respectively. The upstream and downstream probes on the channel electron emitter side are wall emitter probes 4 and 3 (wep4 and wep3), respectively. Both wcp2 and wep4 were located 2.5 cm from the anode, whereas wcp1 and wep3 were 5.1 cm from the anode. These labels and nomenclature are illustrated in both Figs. 2 and 5.

F. Setup and Procedure

The PHT was installed on the AFRL thrust stand in chamber 3. An aluminum mounting plate was attached to the thruster on its front face. The neutralizer was connected to the stand, but not directly to the PHT. It was mounted on the collector side of the PHT as seen in Fig. 3. The experiment was limited to three mass flow controllers, and so both Hall current emitters were supplied by the same 50 sccm controller. The anode used a 250 sccm controller, and the neutralizer cathode used a 20 sccm controller. During testing, each data point took approximately 5 min to record, limited by the speed of the rotary motion of the diagnostic array. No thruster operating parameter (voltage, current, etc.) varied more than 5% during the Faraday probe and RPA sweeps. Overall, the thruster ran stably for over 10 h. The Faraday probe was swept in 180 deg across the centerline of the channel to measure the current density distribution as a function of position, whereas the RPA was positioned on the centerline to record the ion voltage distribution function. The diagnostic array was located in the plane of symmetry of the PHT.

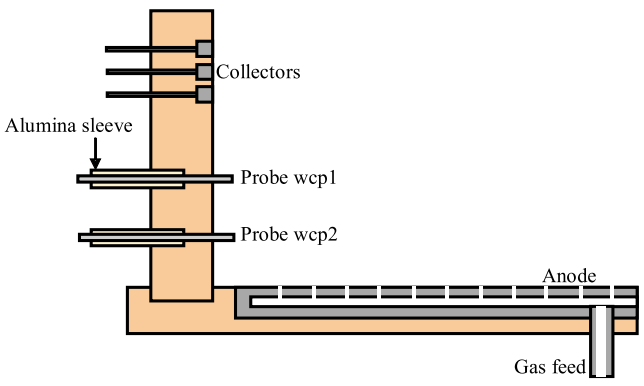

Fig. 5 Cutaway view of the PHT showing anode and wall probe detail.

III. Results

Stable operation of the PHT was obtained for a variety of operational configurations. Discharge voltage was varied between 100–150 V. Larger voltages were not investigated because the thruster Hall current collector electrodes reached thermal limitation. The following sections describe the general operation procedure and the effect of magnetic field variations on thruster operation within this narrow voltage band.

A. Startup and General Operation

PHT operation was accomplished for a variety of experimental configurations and a stable discharge was consistently obtained. Furthermore, the device was operated with the Hall current injected by the emitter cathodes and then collected by the collector electrodes on the opposite side of the channel. This represents the first successful operation of a Hall thruster that recirculates the Hall current across a planar channel. The following paragraphs describe the startup and general operation of the PHT, along with the operating parameters important for this investigation.

The PHT neutralizer and channel emitter cathodes were initially conditioned to prevent poisoning and permanent damage. Current was continuously supplied to the heater of all cathodes during all the experiments. It was determined that the neutralizer cathode would not operate without the heater. Operation of the emitters without heater current was not attempted.

After the cathodes were heated, the neutralizer was ignited by supplying propellant and applying voltage to the igniter electrode. The neutralizer would typically ignite when there was 200 V between cathode and igniter. Neutralizer flow rate was always set at 8 sccm-Xe. The cathode-to-igniter current was set at 0.3 A for all experiments. Larger currents were possible, but the igniter is not designed to maintain the cathode discharge, and overheating the igniter was a concern.

Next, the emitter cathodes were ignited by supplying 25 sccm-Xe (Note that this is total emitter flow rate; we assume it is split 50/50 between the two Hall current emitter cathodes) and applying a potential between each emitter and its corresponding collector electrode across the channel. Emitter 2 (connected to a higher power supply) would ignite first, followed by emitter 1. In general, decreasing or increasing the flow from this optimum value made it more difficult to ignite the emitters. At this point in the startup sequence, plasma was visible across the planar thruster channel. The emitters were operated in both a voltage-limited and current-limited mode. During current-limited operation, increasing emitter flow rate would decrease emitter voltage. In voltage-limited mode, increasing emitter flow rate would increase emitter current. This is standard behavior for any hollow cathode emitter.

The next step in the startup procedure is to apply anode voltage without the magnetic field. As anode voltage increased, anode current increased and the visible plasma shifted toward the exit plane and outside the channel of the thruster. Increasing anode voltage decreases emitter voltage or increases emitter current, depending on whether the emitters are in current- or voltage-limited mode, respectively. The anode voltage is typically increased to 50 V before proceeding with the next step in the startup sequence. At this point, anode propellant flow is not present and not necessary for thruster operation. The discharge is maintained by the emitter flow rate.

Finally, the magnetic field of the thruster is added. As the magnetic field increases (electromagnet current increased), the discharge current decreases. Also, as the magnetic field increases, the emitter voltage increases or current decreases, depending on current- or voltage-limited mode, respectively. At this point, all thruster components are energized and active, and so data collection and study of the system begins.

Table 1 lists the relevant thruster parameters for the operating points important for this paper. Each of the operating configurations is labeled with a thruster point number. For this work, TP13-16 was operated with 100 V discharge voltage, 0 sccm-Xe anode flow rate, 22.5 sccm-Xe emitter cathode flow rate, and different electromagnet currents. TP20-24 is similar to TP13-16 except the anode flow rate

Table 1 Thruster operating points investigated in this work

Thruster point, TP	V_a, V	$Mdot_a$, sccm-Xe	$Mdot_e$, sccm-Xe	I_{emag}, A	B-field, G
13	100	0	22.5	1.0	72
14	100	0	22.5	2.0	129
15	100	0	22.5	2.5	157
16	100	0	22.5	3.0	186
20	100	12.5	22.5	1.5	101
21	100	12.5	22.5	2.0	129
22	100	12.5	22.5	2.5	157
23	100	12.5	22.5	3.0	186
24	100	12.5	22.5	3.5	214
32	150	12.5	14.0	4.5	271
34	150	12.5	14.0	3.5	214
35	150	12.5	14.0	2.5	157
36	150	12.5	14.0	1.5	101

was 12.5 sccm-Xe. Finally, the 150 V discharge voltage case was TP32-36. TP33 is skipped because Faraday probe and RPA results for this thruster operating point were skewed when the thruster experienced a transient during data collection. Table 1 also provides the magnetic field at the exit plane of the thruster in the center of the channel. These field levels are consistent with other types of HETs. Finally, this nomenclature will be used throughout this paper when referring to different PHT operating configurations.

B. Plume Profiles

Faraday probe data sweeps were taken through the plume of the thruster, whereas the RPA was positioned on the centerline to record the ion voltage distribution function. The probes rotate in the plane of symmetry of the PHT and an angular position of 0 deg represents the PHT "centerline." Although the PHT does not have an axis of symmetry, we use the term centerline here to represent the position of the probe when it is 90 deg with respect to the exit plane of the thruster. In this way, we conform to the standard convention used for most state-of-the-art annular HETs [17–19]. Typical plume profile results for the PHT are shown in Fig. 6. These data are for an anode voltage of 100 V, anode flow rate of 12.5 sccm-Xe, emitter flow rate of 22.5 sccm-Xe, discharge current of 3.6 A, electromagnet current of 3 A, and each channel emitter cathode was emitting 0.8 A.

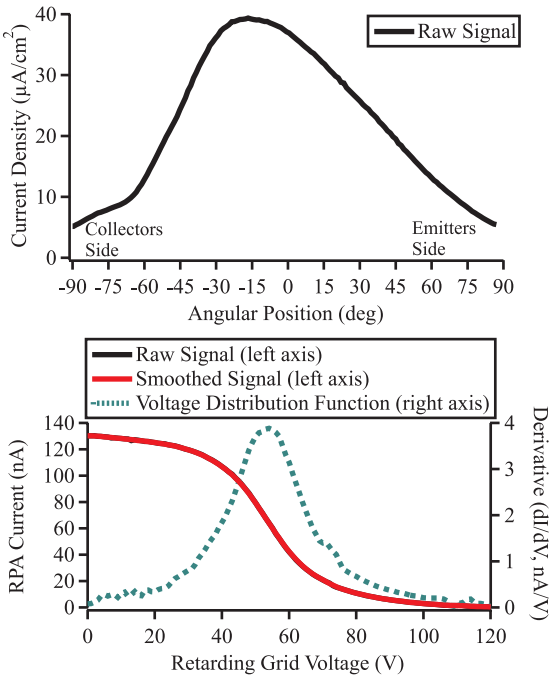

Fig. 6 Example traces from the Faraday probe (top) and RPA (bottom) with the ion voltage distribution function.

For all investigated operating configurations, the plume profile shows a peak at negative angular positions. In Fig. 6, the peak in the current density profile is at approximately −15 deg. Negative angular positions are on the side of the thruster with the collector plates and neutralizer cathode. In the following sections, the angular location at which the peak current density occurs is analyzed as a function of thruster operation. For the RPA data, the peak in the voltage distribution function (i.e., most-probable ion voltage) is shown as a function of thruster operation. The most-probable voltage is the peak in the derivative of the RPA I-V curve and represents the ion voltage that is most likely obtained when randomly sampled. In Fig. 6, the peak in the derivative of the RPA signal occurs at approximately 53 V. Explanations for the nonsymmetric nature of the beam profile are described in Sec. IV.

C. Magnetic Field Effects

The PHT was operated with different magnetic flux densities to analyze the magnetic field effects on thruster operation. In traditional annular thrusters, the magnetic field is set to minimize the discharge current [14,20]. Typically, this yields the best thruster performance. This procedure was attempted, but not realized for the PHT. Specifically, as the magnetic field was increased, the discharge current decreased, but it never reached a minimum. Instead, it continued to decrease with increasing magnetic field. This trend is shown in Fig. 7 with 10% error bars based on the repeatability of the measurements. Data for discharge voltage of 100 and 150 V are shown, with different anode mass flow rates. The thruster point nomenclature is given in Table 1. Note that the decrease in discharge current from the TP13-16 to TP32, 34–36 data is due to a reduction in the channel electron emitter flow rate. The maximum electromagnet current for each data set was limited, due to the thermal limitations of the channel electron collector electrodes, which began to visually show significant thermal load with increasing magnetic field. The authors believe that a minimum discharge current would be found if a sufficient magnetic field were supplied.

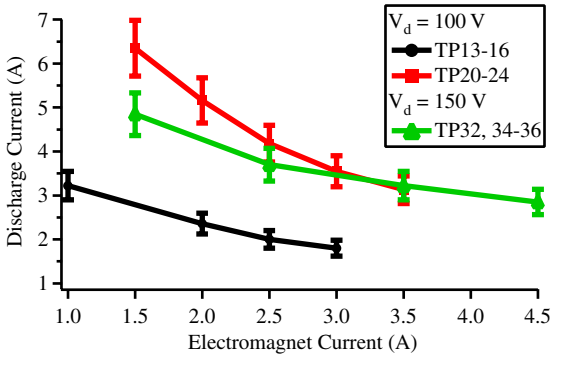

Fig. 7 Discharge current as a function of electromagnet current.

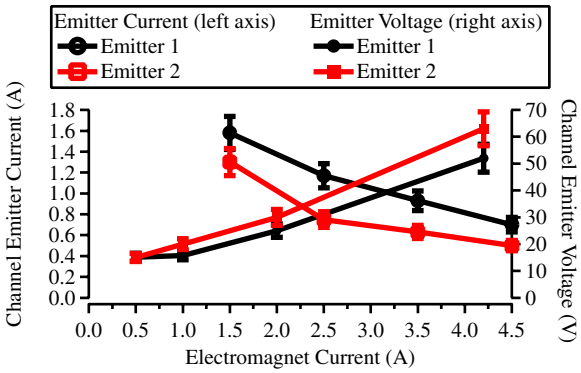

Fig. 8 Emitter operation as a function of electromagnet current.

Figure 8 shows typical trends associated with the channel electron emitters for both constant current (right axis) and constant voltage (left axis) operation. The voltage between both emitter 1–collector 1 and emitter 2–collector 2 was set at constant 2.0 V while the magnetic field was increased. As the magnetic field increases, the emitter current decreases by 50% over the range investigated. Furthermore, emitter 2 current is always lower than emitter 1. In constant current operation, each emitter was set at 0.75 A and the magnetic field increased. As the magnetic field is increased, the voltage increases by a factor of 3 over the range investigated. These results are expected because the transverse magnetic field inhibits electron extraction from the emitter and electron motion across the channel. For the constant voltage case, as the magnetic field increased, the current decreased because fewer electrons had energy sufficient to escape the cathode and enter the discharge channel. Similarly, for the constant current case, as the magnetic field increased, a larger voltage was required to maintain the set electron emission current. The transverse magnetic field acts as an effective barrier to electron injection into and across the channel.

Figure 9 shows channel probe floating potential as a function of magnetic field strength along both thruster walls (refer to Figs. 2 and 4) for two different discharge voltages. For TP13-16, the discharge voltage was 100 V and the floating channel probes record values between 18–60 V. The collector side and emitter side probes record different trends with increasing magnetic field strength. On the collector side of the discharge channel (wcp1 downstream of wcp2), the floating potential decreases as magnetic field increases. Specifically, the upstream probe (wcp2) records a decrease of 20% over the range investigated. For these data points, the emitter–collector circuit was operated in a current-controlled mode. On the emitter side of the thruster channel (wep3 downstream of wep4), the floating potential increases with magnetic field. Specifically, as the magnetic field increases from 1.0 to 3.0 A, probe wep3 shows a gain by a factor of 2.4.

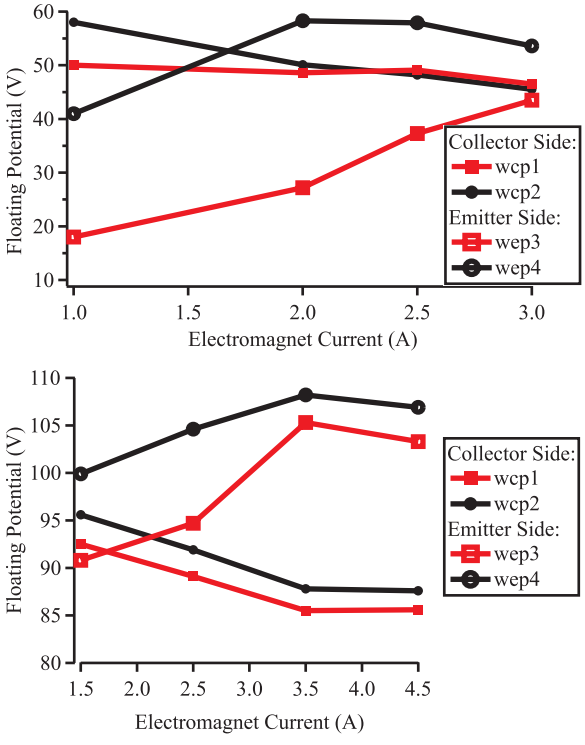

Fig. 9 Channel probe floating potential as a function of electromagnet current for (top) TP13-16 and (bottom) TP32-36.

When the discharge voltage is increased to 150 V for TP32-36, the floating potential increases and is between 85 and 110 V. The same trends are visible. The collector side probes' floating potential decreases with increasing magnetic field, whereas the emitter side probes' floating potential increases with increasing magnetic field. In this case, the collector side probes decrease approximately 10%, and the emitter side probes increase by approximately 10%. It is also important to note that the upstream probes (wep4 and wcp2) record larger floating potentials than the downstream probes for both discharge voltages. For these data points, the emitter–collector circuit is operated in a voltage-controlled mode. This result may be attributed to the fact that the upstream probes are closer to the anode of the thruster. These same trends are recorded for other thruster operating conditions as well.

Figure 10 shows the effect of magnetic field on the ion most-probable voltage, as determined from the RPA data traces on the centerline of the thruster. The most-probable voltage is the peak in the derivative of the RPA I-V curve. Both TP13-16 and TP20-24 are for a discharge voltage of 100 V. At the lowest electromagnet setting, the ion energy is only approximately 68 V, which represents a voltage utilization efficiency of only 68%. Here, the voltage utilization efficiency is defined as the ratio of the most-probable ion voltage to the discharge voltage. State-of-the-art annular HET devices have a voltage utilization on the order of 90% or higher [14]. When the discharge voltage is increased to 150 V for TP32-36, the RPA records ions with an energy of approximately 97 V, resulting in a voltage utilization of about 65%. For all three operating configurations, an increase in magnetic field causes the ion energy to decrease. In fact, the decrease is worst for the TP20-24 operation configuration, with a decrease of 25% over the range investigated. The higher voltage TP32-36 configuration only shows a decrease of 10%, but the range of investigated magnetic field strength is also narrower. The data point for TP32-36 at 1.5 A electromagnet current was only partially obtained because a collector electrode overheated, and so this data point is not reported.

Figure 11 reports the results from the Faraday probe analysis. Specifically, the plume profiles were analyzed and the angular location of the peak in the current density profile was determined. Figure 11 shows the peak location of the current density profile as a function of the electromagnet current. First, we notice that the peak location is always at negative angular positions. Negative angular positions are on the side of the thruster with the collector plates and neutralizer cathode. The second trend we notice is that, as magnetic

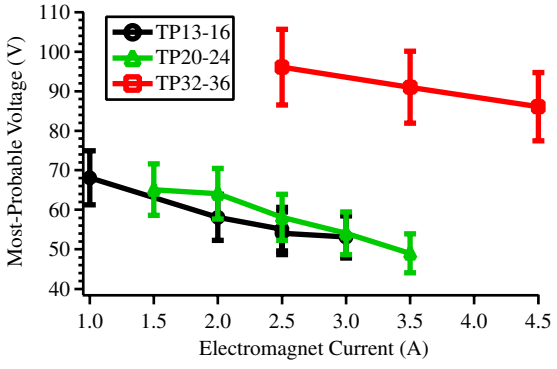

Fig. 10 Most probable ion voltage as a function of electromagnet current.

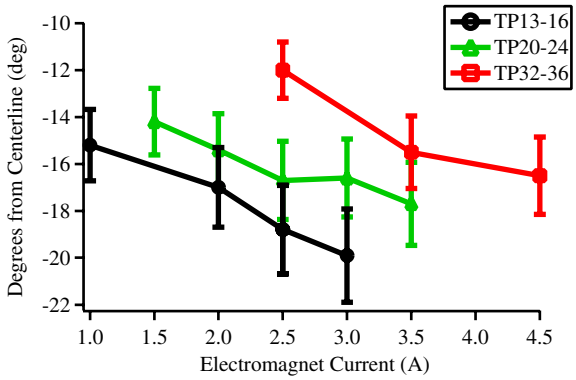

Fig. 11 Plume peak current density angular location as a function of electromagnet current.

field strength increases, the angular position of the current density peak shifts farther from the centerline of the device. In fact, over the range investigated, the peak location can shift up to 4 deg. Finally, the third important trend to notice is that the 150 V discharge case TP32-36 always has a current density peak closer to the centerline of the device. Plume variations across the minor axis of the thruster were not investigated.

The results presented in this section will be used to develop an explanation for the behavior of the beam profile of the PHT. Specifically, the internal probe measurements, most probable ion energy, and current density peak location will be used to explain the trends associated with changes in the magnetic field strength of the thruster.

IV. Discussion

Figure 6 shows that the beam current density is asymmetric and peaked at an angular location off-centerline. For state-of-the-art annular HETs, the current density distribution typically shows a double peak on the centerline, representing each side of the annular channel [14,15]. Ideally, the PHT would show a flat profile that tapers at the wings. We have identified three possible explanations for the nonsymmetric off-centerline peak in current density: 1) nonsymmetric virtual cathode line formation due to electron retardation, 2) space-charge buildup at the collectors, and 3) cross-channel Lorentz force acceleration. In the following paragraphs, we discuss each of these possibilities.

A. Nonsymmetric Cathode Line

Electrons generated in the far field by the neutralizer cathode are inserted into the chamber on one side of the thruster assembly. The local B-field orientation is such that these electrons must collisionally move across field lines to set up the virtual cathode plane where the potential will come to zero. It is conceivable that neutralizer electrons were not able to easily reach the emitter side of the channel, thus setting up a skewed plane of zero potential at the thruster channel exit. The fact that the ion beam angle is slightly skewed toward the cathode neutralizer location suggests that this effect may also be playing a role. Future investigations will relocate the neutralizer cathode on the opposite side of the thruster or below to examine influence on plume divergence.

B. Space-Charge Buildup

The second explanation is based on charge buildup across the channel. As primary electrons leave the emitters and begin Hall drifting across the channel, they have collisions with neutral atoms expelled from the emitters or anode. The products of these collisions are an ion and secondary electron. The ion quickly accelerates out of the thruster because it is unmagnetized, while the primary and secondary electron remain trapped in the Hall drift. As we proceed across the channel, the number of secondary electrons increases because more collisions have occurred between the primary electron and neutral atoms. Because the emitter–collector circuit is closed, any secondary electrons liberated in the acceleration region (i.e., not injected by the emitter cathode) cannot be collected by the collector plates. In other words, the current leaving the emitters must be equal to the current being collected by the collector electrodes on the opposite side. Therefore, excess electrons created by ionization collisions are still trapped by the magnetic field and will be forced to impact the wall and cascade to the anode. Furthermore, the excess electrons that build up on the collector side of the channel may cause more ion production on that side. If this is indeed occurring, one would expect the potential on the collector side to be lower due to the excess electrons. In fact, this is precisely what the experimental evidence shows.

Figure 9 shows that, as the magnetic field increases, the potential on the emitter side of the channel increases, while the collector side potential decreases. As the magnetic field increases, more electrons become trapped in the Hall current and are required to drift across the channel and into the collector sidewall. So, fewer electrons are capable of reaching the emitter side probes, causing the potential to increase. More electrons make it to the collector side, causing the potential to decrease. Therefore, the potential profile across the channel will not be planar and straight, but bowed down near the collectors. This effect will set up an electric field that accelerates ions in both the axial and cross-channel directions. The difference between ideal (no ionization in the acceleration region) and nonideal (collector wall charging) is depicted in Fig. 12.

The consequence of this effect on the plasma beam would be that, as the magnetic field increases, more electrons would build up on the collector side, creating a larger cross-channel electric field. The result would be an acceleration vector that is not purely axial. Therefore, as the magnetic field increases, we would expect the acceleration vector to rotate toward the channel electron collectors and the current density to shift accordingly. This result can be seen in Fig. 11; as the magnetic field increases, the current density shifts farther from the centerline. Finally, if we assume that the contribution of the channel emitter voltage to the ion acceleration is negligible, then the maximum acceleration potential is limited to the anode voltage. Then, another consequence of the acceleration vector rotating away from the centerline is that less ion energy is transferred to the axial direction. This result agrees with Fig. 10, where an increase in the magnetic field causes the most probable ion energy to decrease.

The continuity equation in one dimension can be used to estimate the charge buildup that occurs due to ionizing collisions in the high-B region. This relationship is given in Eq. (1). In this equation, n is density as a function of position, n_o is the initial density, n_b is the background neutral density, σ_{ei} is the electron-impact ionization collision cross section in xenon, x is the cross-channel position, r_L is the Larmor radius, and W is the width of the high-B region. The r_L/L term represents the loss of electrons due to migration across the magnetic field and toward the anode. We assume that, each time an ionizing collision occurs, the primary electron moves across field a distance equal to the Larmor radius. After a sufficient number of collisions, this electron will have escaped the high-B region, which has a width W:

$$\frac{n(x)}{n_o} = \exp\left[n_b \sigma_{\text{ei}} x\left(1 - \frac{r_L}{W}\right)\right] \tag{1}$$

We assume the background neutral density in the PHT channel is 1 mtorr [20], and the electron-impact ionization cross section in xenon is 2.5×10^{-16} cm^2 based on an assumed electron temperature

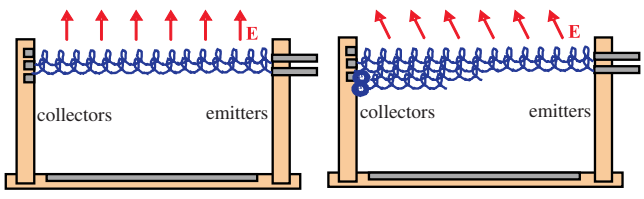

Fig. 12 Ideal operation (left) versus nonideal operation (right).

of 20 eV [21] and collision cross section data reported by [22]. Further, we assume the width of the high-B region is the PHT front pole piece width because experimental magnetic field measurements have shown that the magnetic field decreases outside of this region. A plot of the electron density ratio across the channel is shown in Fig. 13. This analysis shows that the electron density increases across the channel, and the ratio will increase with increasing magnetic field strength. These results are applied next to determine the cross-channel energy imparted to an ion in this region.

We assume that electrons Hall drifting across the channel obey the Boltzmann distribution, and then use the electron density ratio to determine the potential at the edge of the channel (i.e., cross-channel position ~30 cm). The cross-channel energy imparted to an ion can then be calculated using Eq. (2), where E_r is cross-channel energy (electron volts), T_e is electron temperature (electron volts), W is the high-B region width, and L is the length of the cross-channel region. We have also assumed that axial acceleration to the energy measured using the RPA occurs mainly in the high-B region, which is typical for Hall thrusters. Calculations performed with this model are then compared with experimental results

$$E_r = \ell_n\left(\frac{n}{n_o}\right)T_e\frac{W}{L} \tag{2}$$

A simple geometric model can be used to determine the relationship of the axial and cross-channel ion energy with the shift in the current density peak. This relationship is given in Eq. (3), where θ is the angle of the current density peak with respect to the centerline, v_r and v_a are the cross-channel and axial velocity, respectively, and E_r and E_a are the cross-channel and axial energy, respectively:

$$\tan\theta = \sqrt{\frac{E_r}{E_a}} \tag{3}$$

Using the measured axial energy from the RPA data and the measured angular location in the shift of the current density location, it is possible to calculate the cross-channel ion energy. The cross-channel ion energy calculated using experimental data [Eq. (3)] is compared with the cross-channel ion energy calculated assuming charge buildup across the channel [Eq. (2)]. This comparison is shown in Fig. 14a.

The calculated results using the experimental data are shown with 30% error bars, based on the individual error associated with the RPA energy and Faraday probe measurements. The energy calculated assuming charge buildup across the channel is not sufficient to produce the experimental results. The experimental results suggest that a cross-channel energy between 4–7 eV is required to cause the peak current density to shift to negative angular positions. This energy tends to increase with increasing magnetic field strength. Although the same general trend is shown in the model calculations, the magnitude is a factor of 10 too small. Specifically, the charge buildup model only shows a cross-channel energy between 0.54–0.60 eV. However, even though the buildup of charge across the channel may not be contributing to shifting the acceleration velocity vector off-centerline, it may still be contributing to the peaked current density profile.

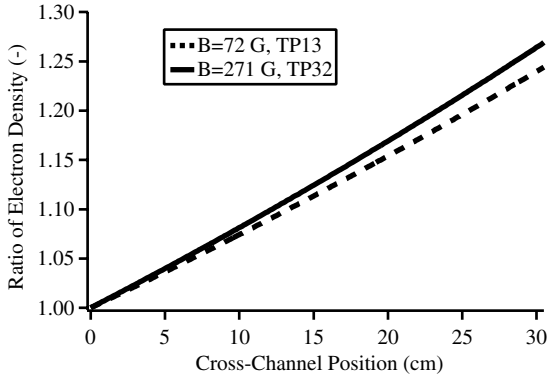

Fig. 13 Electron density as a function of cross-channel position in the PHT.

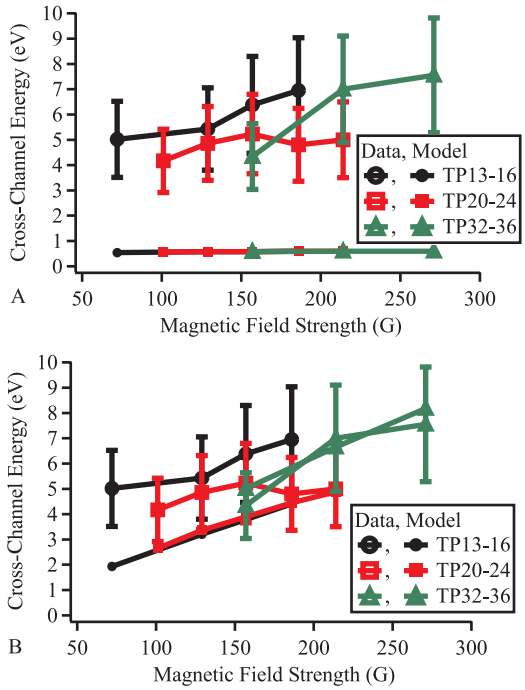

Fig. 14 Comparison of cross-channel energy calculated using experimental data with the a) charge buildup model and b) MHD-effects model.

C. Magnetohydrodynamic Effects

The final explanation to be investigated is magnetohydrodynamic (MHD) effects. An MHD generator operates by passing flowing plasma through two parallel electrodes with a perpendicular magnetic field. The Lorentz force and the orthogonal setup of this geometry cause a potential to appear across the electrodes. This is due to the opposite charge on ions and electrons. In affect, the Lorentz force causes ions to move in the $\mathbf{v}\times\mathbf{B}$ direction, while electrons move in the $-\mathbf{v}\times\mathbf{B}$ direction. This same phenomenon is present in the PHT. As ions move through the high-B region, they experience the Lorentz force. In the following analysis, we examine the cross-channel energy that the Lorentz force can impart to the ions and compare this with the experimental results.

The cross-channel energy imparted to an ion as it passes through the magnetic field is given by Eq. (4), where v is the ion velocity, B is the magnitude of the magnetic field, and W is the high-B region width, which we again assume to be the front pole piece width:

$$E_r = vBW \tag{4}$$

The axial acceleration is assumed to occur over the high-B region width and we use half of the axial energy to account for the acceleration of the ion through this region. With this equation, the calculated cross-channel energy imparted due to the Lorentz force is compared with the experimental calculations, and the result is shown in Fig. 14b. The model results for this MHD case show better agreement with the experiment than the space-charge buildup model. Results for the TP20-24 and TP32-36 cases are within the experimental uncertainty. The TP13-16 case does not fall within the experimental uncertainty but is still a much better match than the space-charge buildup model.

V. Conclusions

Stable operation of a Hall thruster that emits and collects the Hall current in a plane across a linear discharge channel was demonstrated. During this initial test, the PHT was operated at

discharge voltages between 100–150 V to verify operability and stability of the device. Hall current was emitted by hollow cathode electron sources and collected by electrodes on the opposing wall of the thruster. Internal channel wall probes, along with a downstream Faraday probe and RPA, measured changes in thruster plasma as the discharge voltage, magnetic field, and mass flow rates were changed. Results show that most of the plume ions were created in the acceleration zone and obtain energies only 60–70% of the discharge voltage. Further, increasing the magnetic field confines electrons to the Hall-drift region. This causes the discharge current to decrease, but no minimum in discharge current, which traditionally corresponds to an optimum point, was observed.

Plume profiles show a current density peak that is 15–20 deg off-centerline. Ideally, the PHT would have a flat current density profile. An increase in the magnetic field strength causes the current density peak to shift farther from centerline and the most-probable ion energy to decrease. Internal discharge channel floating potentials on the emitter and collector walls show that an increase in magnetic field causes the potential on the emitter side to increase, whereas the collector side potential decreases. A probable explanation of this phenomenon has to do with the increase in trapped Hall current electrons as the field increases. An increase in magnetic field causes more electrons to traverse the channel and reach the collector side, while fewer electrons are capable of remaining on the emitter side of the channel. Although this effect may be causing the peaked current density profile, results indicate that the cross-channel energy imparted to an ion is insufficient to shift the current density peak to the required off-centerline positions. An analysis of MHD effects suggests that the Lorentz force on ions accelerating through the thruster is capable of causing the measured shift in the current density peak. Therefore, it is possible that both of these effects are manifested in the PHT. The build up of trapped space charge across the thruster channel leads to a nonuniform plasma that is accelerated axially by the anode voltage and cross-channel through interaction with the magnetic field.

Acknowledgments

We would like to thank the entire research team at Starfire Industries, LLC, who have been instrumental in this investigation. Also, the testing would not have been possible without the aid of engineers at the U.S. Air Force Research Laboratory, including Dan Brown, James Haas, and Brian Beal. This work was supported by Department of Defense Small Business Innovative Research Phase I contract number FA9300-05-M-3009.

References

[1] Ahedo, E., Gallardo, J. M., and Martinez-Sanchez, M., "Effects of the Radial Plasma-Wall Interaction on the Hall Thruster Discharge," *Physics of Plasmas*, Vol. 10, No. 8, 2003, pp. 3397–3409. doi:10.1063/1.1584432

[2] Meezan, N. B., Hargus, W. A., and Cappelli, M. A., "Anomalous Electron Mobility in a Coaxial Hall Discharge Plasma," *Physical Review E: Statistical Physics, Plasmas, Fluids, and Related Interdisciplinary Topics*, Vol. 63, No. 2, pp. 026410, Feb. 2001. doi:10.1103/PhysRevE.63.026410

[3] Janes, G. S., and Lowder, R. S., "Anomalous Electron Diffusion and Ion Acceleration in a Low-Density Plasma," *Physics of Fluids*, Vol. 9, No. 6, June 1966, pp. 1115–1123. doi:10.1063/1.1761810

[4] Knoll, A., Thomas, C., Gascon, N., and Cappelli, M., "Experimental Investigation of High-Frequency Oscillations Within Hall Thrusters," *42nd Joint Propulsion Conference*, AIAA Paper 2006-5171, 2006.

[5] Keidar, M., and Beilis, I. I., "Electron Transport Phenomena in Plasma Devices with ExB Drift," *IEEE Transactions on Plasma Science*, Vol. 34, No. 3, June 2006, pp. 804–814. doi:10.1109/TPS.2006.874852

[6] Raitses, Y., Staack, D., Keidar, M., and Fisch, N. J., "Electron-Wall Interaction in Hall Thrusters," *Physics of Plasmas*, Vol. 12, No. 5, May 2005, pp. 057104. doi:10.1063/1.1891747

[7] Raitses, Y., Smirnov, A., Staack, D., and Fisch, N. J., "Measurements of Secondary Electron Emission Effects in the Hall Thruster Discharge," *Physics of Plasmas*, Vol. 13, No. 1, Jan. 2006, pp. 014502. doi:10.1063/1.2162809

[8] Schmidt, D. P., Meezan, N. B., Hargus, W. A., and Cappelli, M. A., "Operating Characteristics of a Linear Hall Thruster with an Open Electron-Drift," *35th Joint Propulsion Conference*, AIAA Paper 99-2569, 1999.

[9] Beal, B. E., and Gallimore, A. D., "Development of the Linear Gridless Ion Thruster," *37th Joint Propulsion Conference*, AIAA Paper 2001-3649, 2001.

[10] Hargus, W. A. J., Cappelli, M., "Development of a Linear Hall Thruster," *34th Joint Propulsion Conference*, AIAA Paper 98-3336, 1998.

[11] Linnell, J. A., and Gallimore, A. D., "Internal Plasma Potential Measurements of a Hall Thruster Using Plasma Lens Focusing," *Physics of Plasmas*, Vol. 13, No. 10, Oct. 2006, pp. 103504. doi:10.1063/1.2358331

[12] Kim, V., "Main Physical Features and Processes Determining the Performance of Stationary Plasma thrusters," *Journal of Propulsion and Power*, Vol. 14, No. 5, Sept.–Oct. 1998, pp. 736–743. doi:10.2514/2.5335

[13] Haas, J. M., and Gallimore, A. D., "Internal Plasma Potential Profiles in a Laboratory-Model Hall Thruster," *Physics of Plasmas*, Vol. 8, No. 2, Feb. 2001, pp. 652–660. doi:10.1063/1.1338535

[14] Hofer, R. R., "Development and Characterization of High-Efficiency, High-Specific Impulse Xenon Hall Thrusters," Ph.D. Thesis, Dept. of Aerospace Engineering, Univ. of Michigan, Ann Arbor, MI, 2004.

[15] Brown, D. L., Larson, C. W., Haas, J. A., and Gallimore, A. D., "Analytical Extraction of Plasma Properties Using a Hall Thruster Efficiency Architecture," *30th International Electric Propulsion Conference*, AIAA Paper 2007-188, 2007.

[16] Hutchinson, I. H., *Principles of Plasma Diagnostics*, 2nd ed., Cambridge Univ. Press, Cambridge, England, U.K., 2002.

[17] Rovey, J. L., Walker, M. L. R., Peterson, P. Y., and Gallimore, A. D., "Magnetically Filtered Faraday Probe for Measuring the Ion Current Density Profile of a Hall Thruster," *Review of Scientific Instruments*, Vol. 77, No. 1, Jan. 2006, pp. 013503. doi:10.1063/1.2149006

[18] Walker, M. L. R., Victor, A. L., Hofer, R. R., and Gallimore, A. D., "Effect of Backpressure on Ion Current Density Measurements in Hall Thruster Plumes," *Journal of Propulsion and Power*, Vol. 21, No. 3, May–June 2005, pp. 408–415. doi:10.2514/1.7713

[19] Walker, M. L. R., Hofer, R. R., and Gallimore, A. D., "Ion Collection in Hall Thruster Plumes," *Journal of Propulsion and Power*, Vol. 22, No. 1, Jan.–Feb. 2006, pp. 205–209. doi:10.2514/1.11953

[20] Linnell, J. A., "An Evaluation of Krypton Propellant in Hall Thrusters," Ph.D. Thesis, Dept. of Aerospace Engineering, Univ. of Michigan, Ann Arbor, MI, 2007.

[21] Haas, J. M., "Low-Perturbation Interrogation of the Internal and Near-Field Plasma Structure of a Hall Thruster Using a High-Speed Probe Positioning System," Ph.D. Thesis, Dept. of Aerospace Engineering, Univ. of Michigan, Ann Arbor, MI, 2001.

[22] Kieffer, L. J., and Dunn, G. H., "Electron Impact Ionization Cross-Section Data for Atoms, Atomic Ions, and Diatomic Molecules, I: Experimental Data," *Reviews of Modern Physics*, Vol. 38, No. 1, Jan. 1966, pp. 1–35. doi:10.1103/RevModPhys.38.1

A. Gallimore
Associate Editor